ELSEVIER

Polymer Vol. 37 No. 8, pp. 1329–1338, 1996

0032-3861/96/$15.00+0.00

Rate and temperature dependence of fracture toughness in ABS resins in relation to dispersed-phase structure

L. Castellani
Enichem, Via G. Taliercio, 14-46100 Mantova, Italy

and R. Frassine, A. Pavan and M. Rink*
Politecnico di Milano, P.za L. da Vinci, 32-20133 Milano, Italy
(Received 18 April 1995; revised 8 August 1995)

The paper compares the fracture behaviour of two ABS terpolymers having the same glassy matrix and similar dispersed phase volume, but different amounts of glassy sub-inclusions in the rubbery particles. The fracture toughness of the two materials showed similar strain rate dependence, but different temperature dependence. The results are interpreted in terms of different deformation mechanisms occurring at the failure zone ahead of the crack tip. Copyright © 1996 Elsevier Science Ltd.

(Keywords: toughened polymers; fracture-toughness; yield behaviour)

INTRODUCTION

Investigations on deformation, yield and fracture mechanisms in rubber-toughened polymers have mainly been concentrated on the analysis of the interactions between dispersed-phase domains and the deformation processes occurring in the continuous phase. A distinction is often drawn in the literature between matrix polymers, which, *per se*, usually present brittle behaviour, and those showing ductile behaviour under normal conditions: in the case of brittle matrices, the predominant deformation mechanism is crazing, while in the case of ductile matrices it is shear yielding. 'Simple' systems, in which crazing and shear yielding do not occur simultaneously, have been extensively studied in order to clarify the rubber toughening mechanisms: high impact polystyrene (HIPS) has in most cases been chosen purely as representative of crazing and toughened epoxy resins or toughened nylons as exemplifying shear yielding. Optimum structural characteristics of the second phase domains were found to be different for the two categories of matrix polymers. Particles with a high content of occluded matrix material ('salami particles'), not smaller than a critical size (which for HIPS has been reported to be about 1 μm[1–3], are suitable for crazing matrices[3]; bulk rubber particles are, on the other hand, satisfactory in the case of ductile matrices, provided they are able to cavitate[4–8] and their size and number per unit volume are such that the inter-particle distance is smaller than a critical value[6–9].

According to recent interpretations[10–13], cavitation of the particles plays a key role in the toughening process, not only with ductile matrices, but even when crazing is the dominant mechanism. Cavitation reduces the resistance of the material to dilation, thereby increasing the extent of yielding at the crack tip. Particle cavitation has been documented in different materials, including HIPS, toughened epoxies, toughened PA6.

Acrylonitrile–butadiene–styrene (ABS) materials represent an intermediate case, in which both deformation mechanisms, crazing and shear yielding, may occur in the continuous styrene-acrylonitrile (SAN) random copolymer phase. Due to the simultaneous presence of these deformation processes, optimal characteristics of the dispersed phase are comparatively difficult to establish in this case.

The aim of the experimental work reported on here was to compare the fracture resistance of two ABS samples whose dispersed particles have quite different internal structures.

EXPERIMENTAL

Materials

Two polybutadiene (PB) modified SAN copolymers, named ABS-E and ABS-M, obtained by emulsion and bulk polymerization, respectively, were considered. The two polymerization processes give rise to quite different internal dispersed particle structures, as can be observed in the transmission electron microscope (TEM) micrographs given in *Figure 1*. ABS-E particles contain a very small amount of SAN, occluded in the PB domain, while the ABS-M second phase shows a 'salami' structure with numerous matrix sub-inclusions, very much like HIPS.

To emphasize the effects of the internal structure of the rubber-phase particles, the two samples were chosen as similar as possible as regards SAN matrix, total rubbery phase content, and dispersed particle size. *Table 1* lists the relevant characteristics of the two samples.

* To whom correspondence should be addressed

Molecular weight distribution and the acrylonitrile (AN) content of the SAN matrix are reasonably similar in the two cases.

Overall second phase content was difficult to ascertain because of the very different morphologies of the materials. Commonly used solvent separation methods, which determine the extent of the insoluble phase, may given erroneous results for two main reasons: firstly the shell of grafted SAN surrounding the particles is bound to the rubbery phase (insoluble phase), whereas, from a mechanical point of view, it is to be considered part of the matrix phase; secondly, the matrix resin occluded in the 'salami' particles may be partially extracted during the solution process, thus leading to an underestimation of the amount of rubbery phase.

The dispersed phase volumes shown in *Table 1* were measured by quantitative TEM image analysis, carried out according to a method recently developed in the Enichem laboratories[12].

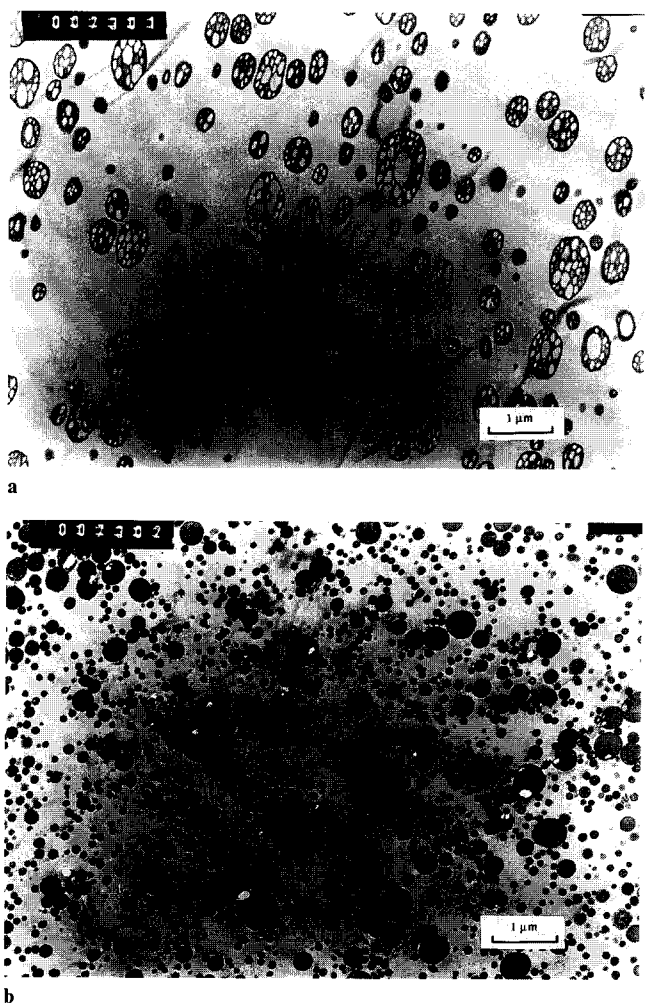

Figure 1 Transmission electron micrographs of (a) ABS-M and (b) ABS-E

Tensile modulus values, measured at 23°C and at a strain rate of $3 \times 10^{-4} s^{-1}$, are reported as an independent check on the validity of dispersed phase content determination. Elastic modulus is indeed known to be affected only by overall second phase content, and not by particle size, provided there is a constant ratio between the effective modulus of the composite particles and the modulus of the matrix[14]. It can easily be calculated (see again ref. 14) that even particles occluding large amounts of glassy resin as in the ABS-M sample have modulus values close to that of PB rubber, at least up to a sub-inclusion content exceeding 90%, which is much higher than in the present case.

Image analysis and tensile modulus data, therefore, both confirm a higher total dispersed phase content in the ABS-E sample, with a difference of not more than 20% between the two samples.

The comparison of PB weight content and second phase volume content makes it possible to estimate the sub-inclusion content of the particles; this is found to be about 6 vol% in ABS-E and 49 vol% in ABS-M (a PB density of $0.9\ g\ cm^{-3}$ was assumed).

Average particle size, shown in *Table 1*, is, in ABS-M, about twice as large as in the emulsion-polymerized sample. The particle size distributions plotted in *Figure 2*, however, span about the same range, from 0.05 to 1 μm, in the two materials. The average size mismatch results from different size distributions, ABS-E showing a relatively sharp peak at about 0.15 μm, whereas ABS-M has a wider distribution, centered around 0.3 μm. A noteworthy consequence of this is that the interparticle distance (IPD) is greater in ABS-M than in ABS-E. A simple equation for the evaluation of the average IPD was proposed by Wu[6]:

$$\mathrm{IPD} = D\left[\left(\frac{\pi}{6\Phi}\right)^{1/3} - 1\right] \qquad (1)$$

in which D is the particle diameter and Φ their volume fraction.

Equation (1) is based on the simplifying assumption that all particles have the same diameter and are regularly arranged in space. IPD values thus obtained are therefore likely to be only rough approximations of the real situation, particularly when broad particle size distributions, like those in *Figure 2*, are considered.

Nevertheless, the average IPD values obtained via equation (1) are reported in *Table 1* for ABS-M and ABS-E as an attempt to quantify the difference between two samples.

In conclusion, the most important structural difference between the two ABS samples investigated here is the

Table 1 Characteristics of materials

	SAN matrix				Dispersed phase			
Material	M_w	M_w/M_n	AN (wt%)	PB (wt%)	Volume (%)	Average diameter (μm)	Average interparticle distance[a] (μm)	Tensile modulus (MPa)
ABS-E	145000	2.8	26.1	24	28.4	0.19	0.04	1930
ABS-M	118000	2.4	26.4	10.8	23.4	0.39	0.12	2150

[a] See text

sub-inclusion content of the dispersed phased. Particle size range is similar in the two materials, although there is a difference in the particle size distribution which gives rise to a significant difference in the average interparticle distance.

Tensile tests

Tests were performed on dumb-bell specimens 3 mm thick, 5 mm wide and with a gauge length of 20 mm, at temperatures between −60 and 70°C and displacement rates ranging from 0.1 mm min^{-1} to 1 m s^{-1}. A 12.5 mm clip gauge was used to measure the true strain on the sample. Yield stress was taken at the maximum on the stress–strain curve. In a few cases, no maximum was observed and yield stress was taken as the stress at which a constant true strain rate begins. This condition was chosen since it was found to occur at the maximum stress when a maximum is observed.

Measurements at 1 m s^{-1} were performed without an extensometer, and thus true strain and true strain rate were not obtained in these tests; however, a maximum in the stress-*versus*-time curve was observed, and the yield stress was therefore taken at this point.

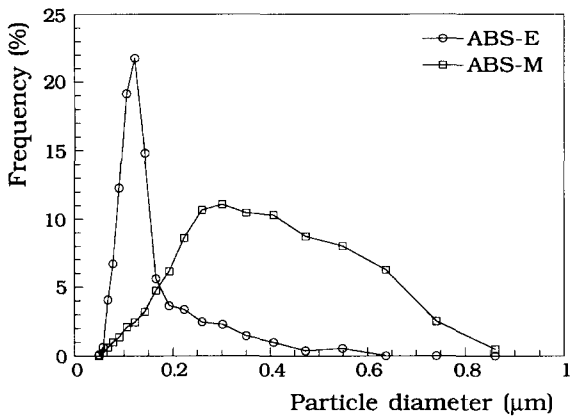

Figure 2 Particle size distribution for ABS-M and ABS-E

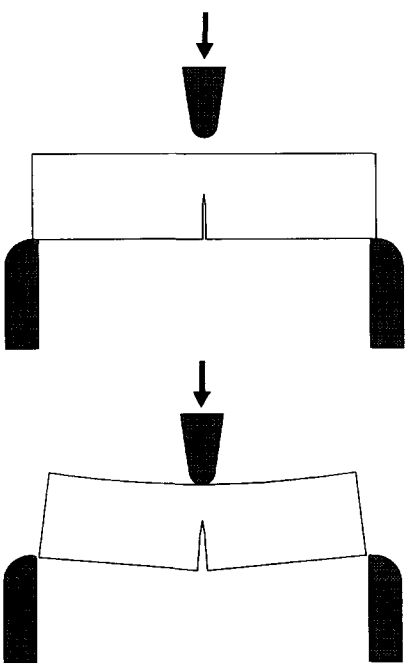

Figure 3 Experimental configuration for *J* resistance tests at high rates

Fracture tests

J-resistance curves and *J* conventional values for fracture initiation, $J_{0.2}$, taken at 0.2 mm crack advance, were determined according to ref. 15. Single edge notched [SE(B)] 10 × 20 × 90 mm specimens were tested in the three-point bending configuration, with an $S = 80$ mm span. Notches were introduced by alternatively sliding a sharp blade (tip radius ~ 10 μm) scapel-wise to a depth corresponding to a crack length specimen width ratio, a/W, of 0.6.

Tests were carried out at 1 mm min^{-1} and 1 m s^{-1} at 23°C and −50°C on both materials, and also at 10 and 100 mm min^{-1} at 23°C on ABS-M.

Slow rate tests (1–100 mm min^{-1}) were carried out on a screw-driven Instron dynamometer. High rate tests (1 m s^{-1}) were performed using an instrumented dart drop tower, Fractovis 6789/050 by CEAST.

In the case of the slow rate tests, the different crack advancements needed to determine the *J* resistance curve were obtained by loading test specimens having identical notch length up to different displacements, and then unloading them at a rate at least 10 times the loading rate. The specimens were finally broken open at an even higher rate.

For the high rate tests we adopted a different

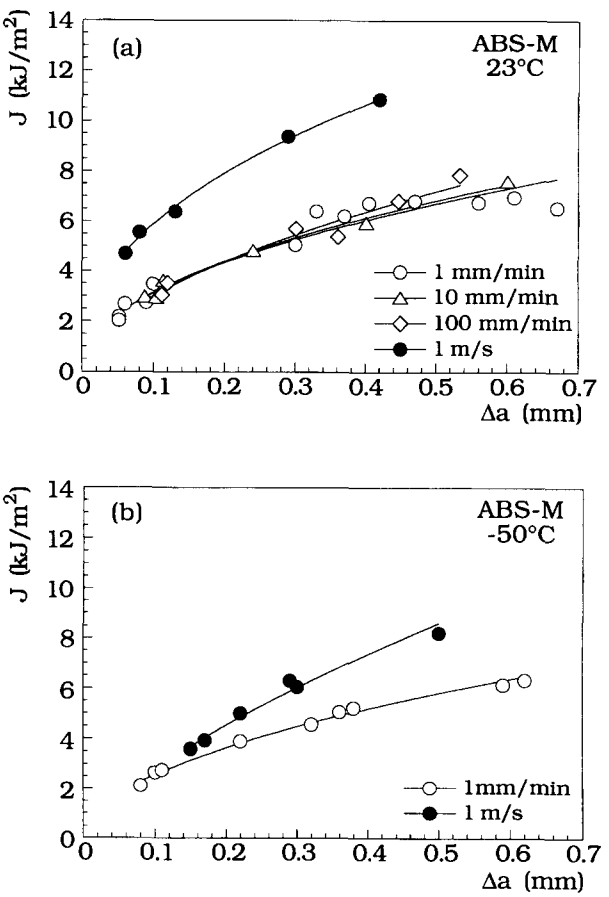

Figure 4 *J* resistance curves of ABS-M at (a) 23°C and (b) −50°C

procedure. Test specimens with the same initial notch length were machined to varying lengths L just a little wider than the test span, S, so that each specimen could be deflected during the test up to the point when it slipped off the supports. (Special care is required to position the specimen symmetrically on the bending rig.) By slightly varying the length of the specimens different deflections (and thus different crack growths) are obtained before the slipping off from the support (*Figure 3*). Complete rupture was then again obtained by striking the specimen at a rate higher than that of the test.

At all testing rates, crack growth could easily be ascertained on the fracture surface after the test. These readings, as suggested in ref. 15, were checked by cutting some of the specimens halfway through their thickness, polishing the cut surface, and then measuring the crack growth from the side.

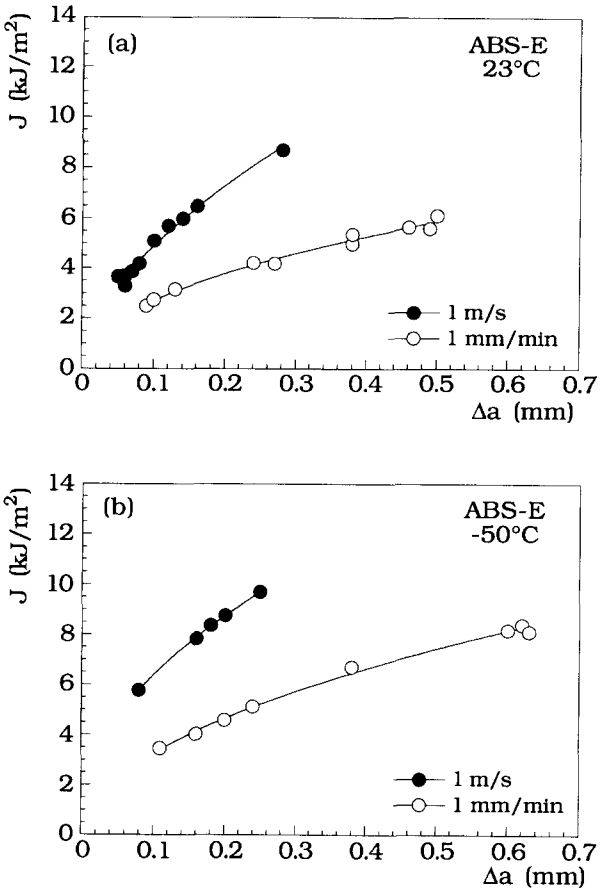

Figure 5 J resistance curves of ABS-E at (a) 23°C and (b) −50°C

RESULTS AND DISCUSSION

Fracture toughness

Figures 4 and *5* show the resulting J-resistance curves at 23°C and −50°C at the different displacement rates, $\dot{x}$, for the two materials, respectively. In the literature, various trends in fracture toughness as a function of rate and temperature for these types of materials can be found[16–18]. In this work, both materials tested turned out to be more resistant at $1\,m\,s^{-1}$ than at $1\,mm\,min^{-1}$ at both temperatures considered. With ABS-M at 23°C, for which tests were also carried out at other deformation rates, it may be observed that J_R curves are substantially identical for $\dot{x}$ in the range from $1\,mm\,min^{-1}$ up to $100\,mm\,min^{-1}$, after which the curve rises at $1\,m\,s^{-1}$. As for temperature dependence, the two materials show opposite trends: when the temperature is changed from 23°C to −50°C , ABS-E becomes more, and ABS-M less resistant.

For discussion of the temperature and rate effects on the resistance of these materials, reference will be made to the values of J at 0.2 mm crack extension. These have been obtained from the relevant J-resistance curves and are given as a function of rate and temperature in *Figures 6* and *7*.

In view of the highly ductile fracture behaviour of these materials, suggesting that major plastic deformations take place in the process zone surrounding the crack tip, the rate and temperature dependence of fracture toughness may be thought to be directly related to the yield

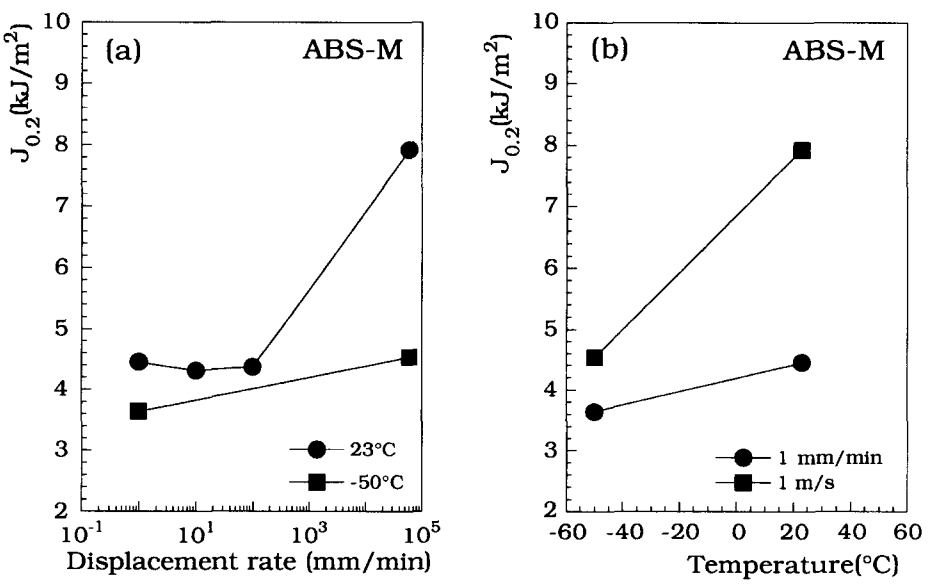

Figure 6 $J_{0.2}$ as a function of (a) displacement rate and (b) temperature for ABS-M

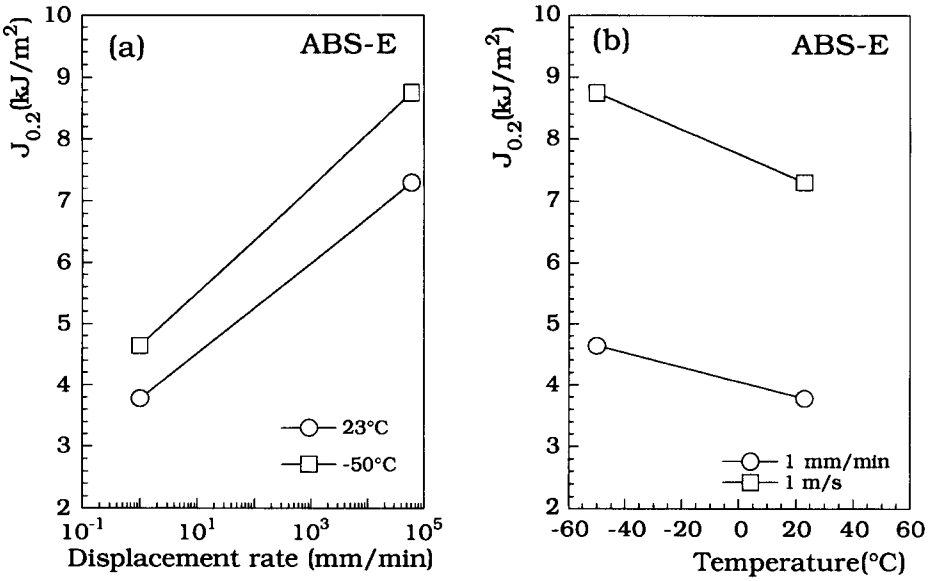

Figure 7 $J_{0.2}$ as a function of (a) displacement rate and (b) temperature for ABS-E

behaviour of the material—at least as an initial approximation.

The tensile yield stress values of the two materials at the temperatures and displacement rates considered for the fracture tests are shown in *Figures 8* and *9*. These results show clearly that the rate and temperature dependence of fracture is not determined only by the rate and temperature dependence of σ_y. For example, let us consider the rate dependence in the case of ABS-M at 23°C: $J_{0.2}$ (*Figure 6a*) is nearly constant for rates between 1 and 100 mm min^{-1} and then increases between 100 mm min^{-1} and 1 m s^{-1}, whereas the yield stress increases steadily over the whole range of rates considered (*Figure 8a*). Furthermore, the temperature-dependence of the fracture resistance shows opposite trends in the two materials (*Figures 6b* and *7b*), while yield stress shows a regularly decreasing trend with increasing temperature for both materials (*Figures 8b* and *9b*).

We will therefore draw a distinction between the two separate contributions to fracture toughness made by two different zones at the crack tip: the process zone, in which non-linear and/or yield phenomena occur, and a failure zone, which may be thought of as a relatively small volume contained in the other, which undergoes substantial deformations before material separation occurs.

In this connection, it is appropriate to recall that the toughness J can be considered as being proportional to the product of the yield stress, σ_y, by the crack opening displacement, δ (see for example ref. 19)

$$J \div \sigma_y \delta \tag{2}$$

By doing so, we can consider the effect of the yield stress, which controls the dimension of the process zone, separately from that of δ, which is more directly related to the stretching phenomena occurring in the failure zone.

While it was possible for the yield stress to be directly measured, δ was not. As a first approximation let us

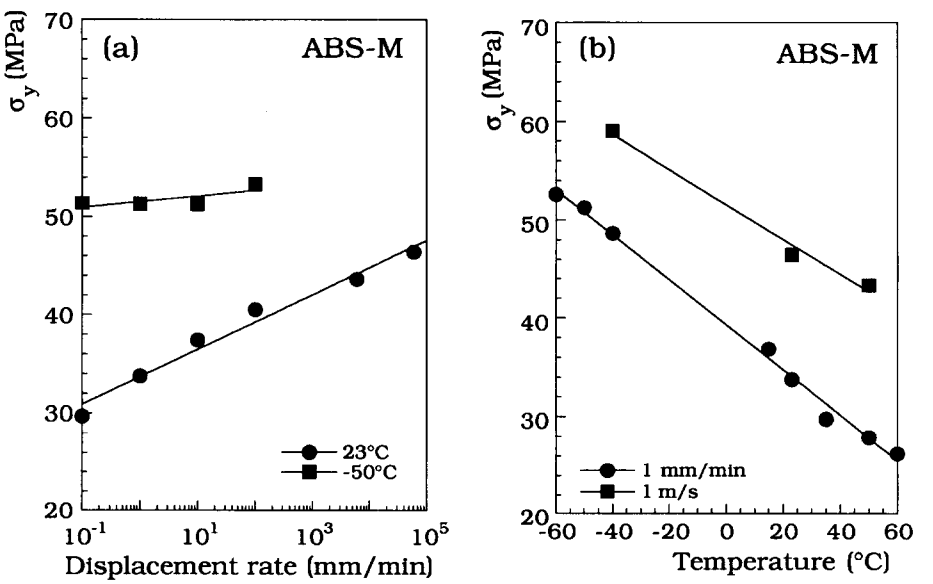

Figure 8 Tensile yield stress, σ_y, as a function of (a) displacement rate and (b) temperature for ABS-M

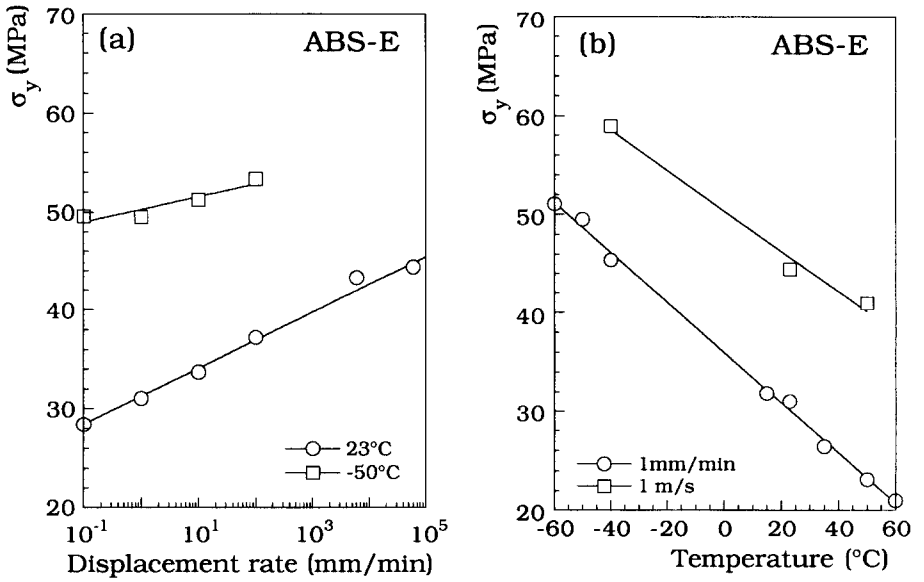

Figure 9 Tensile yield stress, σ_y, as a function of (a) displacement rate and (b) temperature for ABS-E

consider, instead of the crack opening displacement, δ, the load point displacement, x, which may be assumed to be proportional to δ[20]. We will thus examine the rate and temperature dependence of $x_{\Delta a=0.2}$, i.e. the value of the load point displacement measured at the same crack advancement at which $J_{0.2}$ is determined. This quantity can easily be obtained from the experimental data obtained during J testing. *Figure 10* shows, as an example, the load point displacement *versus* crack advancement data obtained in the J tests performed on ABS-M at 23°C at different displacement rates. Experimental points were interpolated and the $x_{\Delta a=0.2}$ values were thus obtained. It is worth noting that there is an inversion in the location of the curves in *Figure 10* when the rate is changed from 100 mm min^{-1} to 1 m s^{-1}.

Figures 11 and *12* show $x_{\Delta a=0.2}$ as a function of rate and temperature for ABS-M and ABS-E, respectively. For ABS-M at 23°C (*Figure 11a*), $x_{\Delta a=0.2}$ shows a minimum for 100 mm min^{-1} (as was already observed in *Figure 10*). As this result confirms, the trends observed for $J_{0.2}$ (*Figure 6a*) seem indeed to reflect the product of the quantities σ_y and $x_{\Delta a=0.2}$ (*Figures 8a* and *11a*) as expected from equation (2). The minimum observed in $x_{\Delta a=0.2}$ *versus* displacement rate (*Figure 11a*) could be attributed to local adiabatic heating at the crack tip (failure zone), occurring at the higher rates[22].

The different temperature dependence of $J_{0.2}$ exhibited by ABS-M and ABS-E at both rates examined (*Figures 6b* and *7b*) also seems to reflect the different trends of $x_{\Delta a=0.2}$ (*Figures 11b* and *12b*), since σ_y whose the same decreasing trend with increasing temperature for both materials (*Figures 8b* and *9b*). This indicates that probably different local deformation mechanisms occur in the two materials as temperature changes.

From these results it appears that the fracture toughness, $J_{0.2}$, of these two materials is determined not only by the behaviour of the yielding material in the process zone, but also by the local deformation mechanisms occurring in the failure zone near the crack tip. While yield behaviour as a function of rate and temperature appears to be similar in the two materials, the local deformation mechanisms (as reflected by $x_{\Delta a=0.2}$) seem quite different.

Direct observation of the plastic deformation processes occurring in the failure zone, which might support the above findings and relate the differences observed to the structure of the dispersed particles, is hindered by considerable experimental difficulties.

We therefore carried out, instead, a set of dynamic mechanical experiments and a careful analysis of the rate and temperature effects on yielding. The results of these investigations, described below, disclosed the existence of different residual stresses in the matrix surrounding the second-phase particles in the two materials and different deformation processes in progress in the two cases.

Dynamic–mechanical measurements

Two series of samples with varying rubber content were prepared by diluting the original ABS-M and ABS-E with varying amounts of styrene-acrylonitrile resin (SAN). Molecular weight distributions of the added SAN and of the matrices of the original ABS materials were closely matched. Mixing was carried out in the molten state.

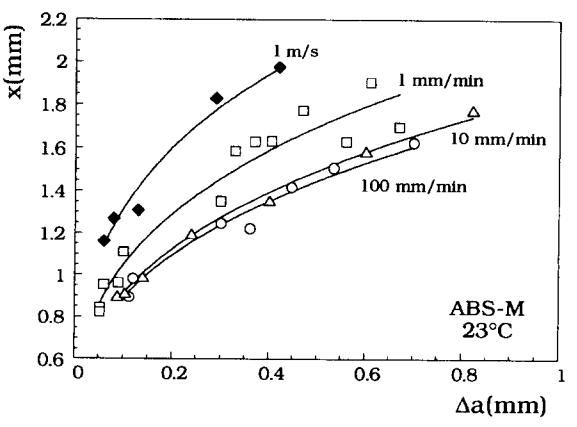

Figure 10 Load point displacement, x, as a function of crack growth, Δa, for different displacement rates for ABS-M at 23°C

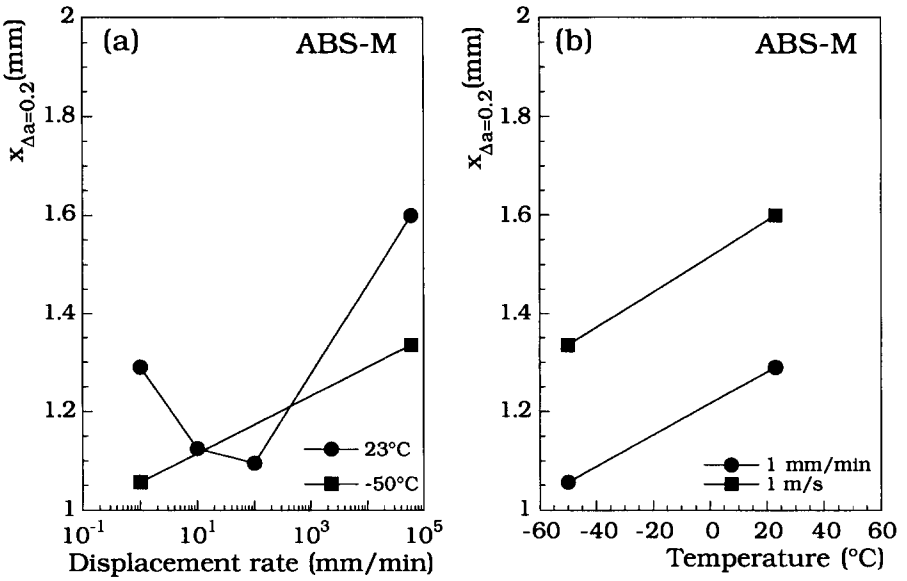

Figure 11 Load point displacement at 0.2 mm crack growth, $x_{\Delta a=0.2}$, as a function of (a) displacement rate and (b) temperature for ABS-M

The two ABS series were subjected to dynamic mechanical analysis, carried out on compression-moulded specimens in three-point bending geometry by means of a Rheometrics RSA II. The frequency of the forced sinusoidal oscillations was 1 Hz and the imposed maximum strain was 0.03%.

Figure 13 shows the tan δ *versus* temperature curves obtained from these tests, in a temperature range around the glass transition of the rubber phase.

The position of the tan δ maximum, representative of the glass transition of the PB rubber, is not affected by its content in the samples of the ABS-M series; conversely, in the case of ABS-E, an appreciable shift to lower temperatures is observed with decreasing rubber content.

Moreover, at the lowest rubber content in the ABS-E series, a splitting of the tan δ peak into two smaller ones is noticed.

Similar dynamic mechanical behaviour was observed in emulsion ABS samples by Morbitzer *et al.*[21], and was explained by the thermal stresses arising from the thermal expansion coefficient mismatch of the two phases. Rubber, which has the higher thermal expansion coefficient, undergoes dilational hydrostatic stress when the material is cooled below the glass transition temperature of the SAN phase, and this accounts for the peak shift observed.

The increase in peak shift with decreasing rubber content observed can also be explained in view of the level of the thermal stresses built up. This will be proportional to the difference in the thermal expansion coefficient $\Delta\alpha$ between the particle and the surrounding medium. If the particle were isolated, the surrounding medium would consist of pure matrix. Even at moderate rubber particle concentrations, however, the effect of the neighbouring particles cannot be ignored: the medium surrounding one particle is, in fact, the particulate composite material. Its thermal expansibility (α_c) is, indeed, intermediate between those of the two components, the

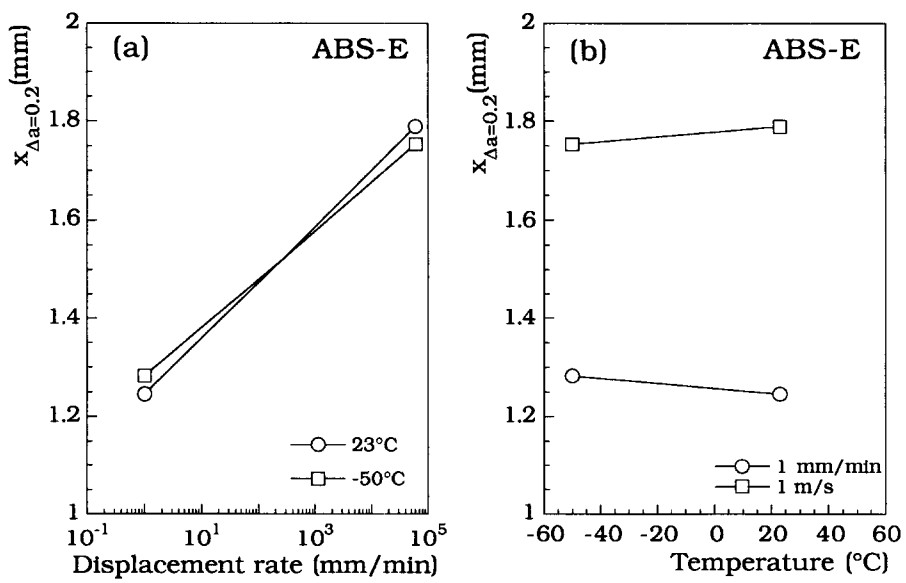

Figure 12 Load point displacement at 0.2 mm crack growth, $x_{\Delta a=0.2}$, as a function of (a) displacement rate and (b) temperature for ABS-E

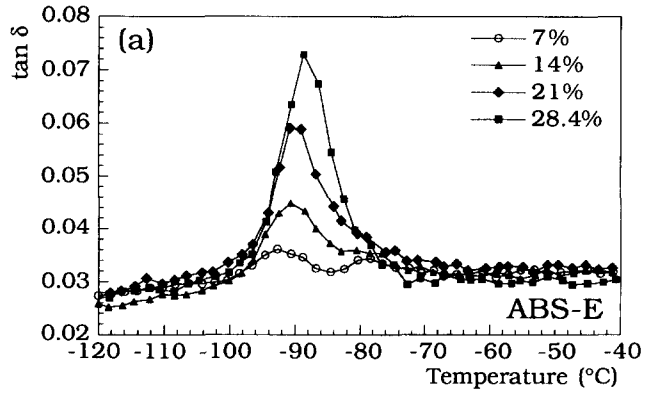

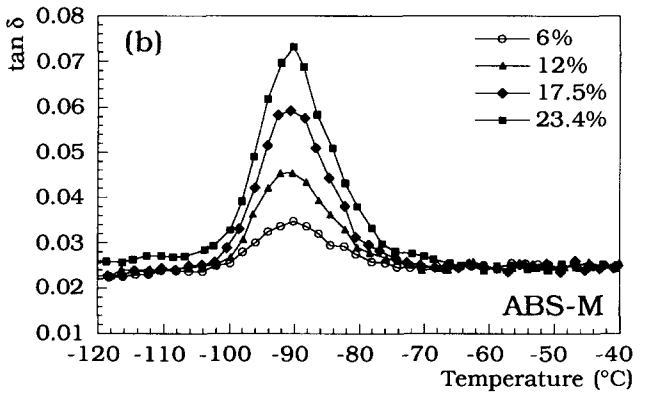

Figure 13 Loss tangent, tan δ, as a function of temperature for ABS samples generated from (a) ABS-E and (b) ABS-M, with different second phase volume contents

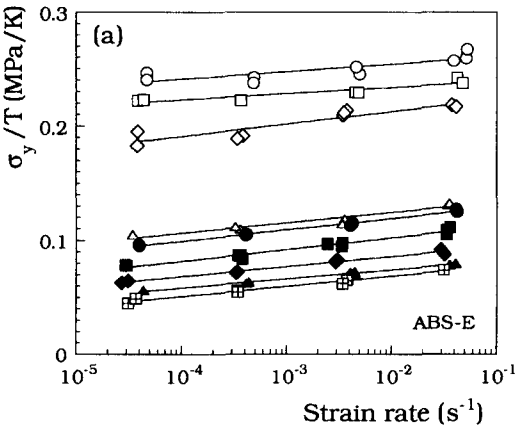

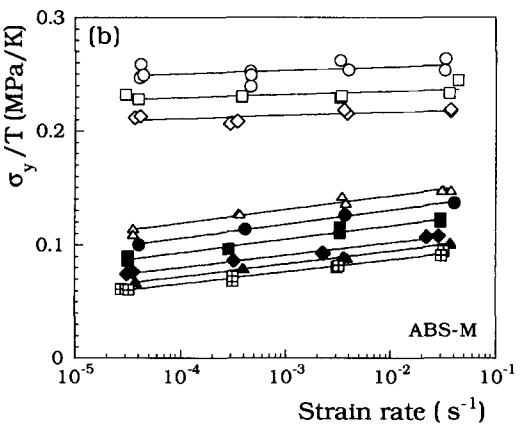

Figure 14 Tensile yield stress, σ_y, plotted as a function of strain rate according to Eyring's equation for (a) ABS-E and (b) ABS-M. ⊞ −60°C, ▲ −50°C, ◆ −40°C, ■ 15°C, ● 23°C, △ 35°C, ◇ 50°C, □ 60°C, ○ 70°C

particles (α_p) and the matrix (α_m), depending on their proportion. As the particle concentration decreases, the effective thermal expansion coefficient of the ABS composite (α_c) gets closer to that of the SAN matrix (α_m) and the difference $\Delta\alpha = \alpha_p - \alpha_c$ increases, thus raising the thermal stresses and their effect on the tan δ peak position.

The difference between the two materials, ABS-E and ABS-M, observed in *Figure 13* can be explained by considering their differences in particle composition and structure. Pavan and Ricco[23] calculated how the dilational stress in the rubber particle is decreased if rigid sub-inclusions are present. SAN matrix inclusion content is high in ABS-M, and the overall thermal stresses are therefore negligible, giving no apparent peak shift as shown in *Figure 13b*.

Peak splitting was also reported by Morbitzer *et al.*[21], and the phenomenon was ascribed either to particle-matrix interfacial debonding or to 'scission effects inside the rubber particles' under the high thermal stress levels found at very low rubber contents. As later pointed out by Booij[24], the hydrostatic stress inside the particles may reach values of the order of 50 MPa, which may be sufficient to initiate a stress-activated cavitation inside the rubber. A typical value for the bulk modulus of PB rubber is 2000 MPa[11,24]; therefore, under conditions in which peak splitting is observed, volume strains greater than 2% may be reached. According to the recent model for particle cavitation in rubber-toughened plastics proposed by Bucknall *et al.*[11], such a value of volume strain is high enough to make particles as small as 0.1 μm in radius cavitate even under the most unfavourable conditions (high shear modulus and high surface tension of the rubber). Rubber cavitation is therefore an acceptable explanation for the peak-splitting observed, and a general enhancing effect of the thermal stress on the cavitation of the rubber particles is to be expected.

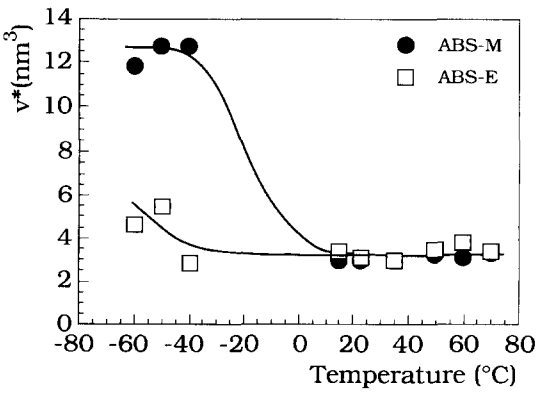

Figure 15 Activation volume, v^*, as a function of temperature for ABS-M and ABS-E

A substantial difference therefore exists between ABS-E and ABS-M as far as the stress fields inside the particles and in the immediate neighbourhood of the particles themselves is considered. Moreover, cavitation of the rubber particles under the action of an externally applied stress is more likely to occur in ABS-E than in ABS-M, due to the superimposed thermal stress discussed above. Cavitation, as recently pointed out by many authors[3–5,7–10,25], strongly affects the yielding micromechanisms in rubber-toughened polymers giving rise to considerable enhancement in fracture toughness.

Yield measurements

Differences in the yielding mechanisms may be detected by considering the rate and temperature-dependence of the yield stress. The tensile test data in *Figures 8* and *9* have therefore been completed, especially in the low strain rate range, for a better evaluation of the yielding kinetics. Plots of σ_y/T *versus* log ($\dot{\epsilon}$), T being the absolute temperature and $\dot{\epsilon} = d\epsilon/dt$ the strain rate for the two materials, are shown in *Figure 14*.

Quantitative treatment of these data may be accomplished by means of the well known Eyring equation (see ref. 1):

$$\frac{\sigma_y}{T} = \frac{2\Delta H}{\gamma \nu^* T} + \frac{2R \cdot 2.303}{\gamma \nu^*} \log_{10}\left(\frac{\dot{\epsilon}}{\dot{\epsilon}_0}\right) \qquad (3)$$

in which R is the gas constant, ΔH the activation energy, ν^* the activation volume, and γ a 'stress concentration' factor that takes into account the dependence of the yield stress on the second phase content, calculated here by means of the expression attributed to Ishai and Cohen[26]

$$\gamma = (1 - 1.21\Phi^{2/3})^{-1} \qquad (4)$$

The application of equation (3) to the experimental data in *Figure 14* produces the temperature dependence of the activation volume given in *Figure 15*. Similar ν^* values are found for the two materials in the high temperature range (from about 15 up to 70°C), while at low temperatures (−60 to −40°C) the activation volume is higher for ABS-M. Previously[27] for ABS type materials differences in the activation volume have been associated to different deformation mechanisms taking place during yielding. The results reported in *Figure 15* then suggest that probably in the two materials different deformation mechanisms are active at low temperatures.

From the results of dynamic-mechanical and yield tests a direct association may be assumed between the thermal stress differences, due to the different sub-inclusion content of the two materials and the appearance of different deformation mechanisms at low temperature. Thermal stress effects are indeed enhanced in the low temperature range.

Particle size distribution can also affect the deformation processes. In the present case, even if the size range of the rubber particles is similar in the two materials, the different distributions give rise to different average inter-particle distance (IPD) values: IPD has been shown to be an important parameter, mainly with reference to shear yielding processes[6,7].

The effect of the IPD has been reported to be that of determining a transition between a ductile behaviour (occurring for IPD lower than a critical value) and a brittle behaviour (occurring above the critical IPD)[6]. It is reasonable to expect that the critical IPD for the ductile-brittle transition is temperature dependent, and therefore similar materials having different IPD (like the two ABS samples here considered) are expected to show ductile brittle transitions at different temperatures. This could explain the fact that ABS-M becomes brittle when cooled to −50°C, while ABS-E does not. However, this cannot explain the fact, here experimentally observed, that ABS-E is tougher at −50°C than at 23°C.

For these reasons we consider that the opposite temperature dependencies for toughness observed for ABS-E and ABS-M cannot be the effect of the existing IPD difference. We propose therefore that the *J versus* temperature results are directly related to the thermal stress differences due to the different sub-inclusion content in the particles of the two samples.

CONCLUSIONS

Two ABS samples have been considered, ABS-E and ABS-M, having similar SAN matrix molecular structure and total dispersed phase content, but with very different internal particle structure, namely bulk rubber in ABS-E and a highly occluded 'salami' structure in ABS-M.

Particle size range is also similar in the two cases, but the size distributions are different, with a prevalence of relatively small particles ($\sim 0.15\,\mu$m) in ABS-E and a wider distribution centered at about $0.3\,\mu$m, in ABS-M.

J-integral evaluation of fracture toughness was carried out at various load point displacement rates and temperatures. Although comparable rate dependencies of J were found for the two samples, the effects of temperature were different, the toughness of ABS-E being higher at low temperatures than at high ones and the opposite occurring for ABS-M.

Two contributions to the fracture toughness were assumed: the yielding of the material in the 'process zone' surrounding the advancing crack, and the large plastic deformations eventually leading to material separation in a smaller 'failure zone' nearest to the crack tip. Since the tensile yield stress rate and temperature dependencies were found to be similar in the two samples, the differences in fracture toughness observed were ascribed to different behaviour in the failure zone.

Investigations aimed at clarifying the possible relationships between particle morphology and plastic deformation processes were then carried out separately, in two different ways: by dynamic mechanical experiments and through a study of kinetics of plastic deformation.

By means of dynamic mechanical experiments, evidence was found of the marked effects of particle structure on the mechanical stress fields inside the particles and in the matrix surrounding them. Thermal stresses, arising from the thermal expansion mismatch between glassy matrix and rubber, were shown to be negligible in ABS-M due to the high sub-inclusion content, and were found, conversely, to be much higher in ABS-E. Moreover, cavitation of the rubber particles caused by the thermal stresses was observed in ABS-E at low temperatures and low rubber contents.

Yield stress data at various rates and temperatures

were analysed by the Eyring approach, and the activation volume was determined as a function of temperature. The same activation volume for the two materials was found at room temperature, while at low temperatures the activation volume of ABS-M was higher than that of ABS-E. Despite the similarity of the yield stress levels, therefore, the presence of different deformation kinetics was confirmed.

The different temperature dependence observed in fracture toughness for the two materials can therefore be related to the presence of different deformation processes at low temperatures.

Although the two materials examined have different particle size distribution and interparticle distance, which may affect the nucleation and evolution of the deformation micromechanisms, we ascribe their different behaviour at low temperatures to the internal particle structure affecting the elastic stress field in the material and causing the cavitation of the particles in ABS-E.

REFERENCES

1 Bucknall, C. B. 'Toughened Plastics', Applied Science, London, 1977
2 Bucknall, C. B. in 'Polymer Blends' (Eds D. R. Paul and S. Newman), Academic, New York, 1978
3 Donald, A. M. and Kramer, E. J. *J. Appl. Polym. Sci.* 1982, **27**, 3729
4 Yee, A. F. and Pearson, R. A. *J. Mater. Sci.* 1986, **21**, 2462
5 Yee, A. F. and Pearson, R. A. *J. Mater. Sci.* 1986, **21**, 2475
6 Wu, S. *Polymer* 1985, **26**, 1855
7 Borggreve, R. J. M., Gaymans, R. J., Schuijer, J. and Ingen Housz, J. F. *Polymer* 1987, **28**, 1489
8 Borggreve, R. J. M., Gaymans, R. J. and Schuijer, J. *Polymer* 1989, **30**, 71
9 Borggreve, R. J. M., Gaymans, R. J. and Eichenwald, H. M. *Polymer* 1989, **30**, 78
10 Lazzeri, A. and Bucknall, C. B. *J. Mater. Sci.* 1993, **28**, 6799
11 Bucknall, C. B., Karpodinis, A. and Zhang, X. C. *J. Mater. Sci.* 1994, **29**, 3377
12 Guild, F J. and Kinloch, A. J. *J. Mater. Sci.* 1995 **30**, 1689
13 Nielsen, L. E. 'Predicting the Properties of Mixtures', Marcel Dekker, New York 1978
14 European Structural Integrity Society (ESIS), Technical Committee 4 'Polymers and Composites', 'A Testing Protocol for Conducting J-Crack Growth Resistance Curve Tests on Plastics', March 1992
15 Gaggar, S. K., Wilson, J. R. in 'Proc. Intl. Conf. Toughening of Plastics I', July 1978, Plastics and Rubber Institute, London, p. 17
16 Sridharan, N. S. and Broutman, L. J. in 'Proc. Intl. Conf. Toughening of Plastics I', July 1978, Plastics and Rubber Institute, London, p. 19
17 Riccò, T., Rink, M., Caporusso, S. and Pavan, A. in 'Proc. Intl. Conf. Toughening of Plastics II', July 1985, Plastics and Rubber Institute, London, p. 27
18 Turner, C. E. in 'Post-Yield Fracture Mechanics', 2nd Edn, Elsevier, London 1984, Chap. 2, p. 60
19 Elliott, D. and May, M. J. British Iron and Steel Association, open report MG/C/48/69, 1969
20 Morbitzer, L., Kranz, D., Humme, G. and Ott, K. H. *J. Appl. Polym. Sci.* 1976, **20**, 2691
21 Williams, J. G. 'Fracture Mechanics of Polymers', Ellis Horwood, Chichester, 1985, p. 270
22 Pavan, A. and Riccò, T. *J. Mater. Sci. Lett.* 1976, **11**, 1180
23 Booij, H. C. *Br. Polym. J.* 1977, 47
24 Dijkstra, K., Van der Wal, A. and Gaymans, R. J. *J. Mater. Sci.* 1994, **29**, 3489
25 Ishai, O. and Cohen, L. *J. Compos. Mater.* 1968, **2**, 302
26 Sultan, J. N. and McGarry, F. J. *Polym. Eng. Sci.* 1974, **14**, 282